J Appl Electrochem (2012) 42:471–475
DOI 10.1007/s10800-012-0421-5

ORIGINAL PAPER

Self-standing integrative cell with an inorganic separator for lithium-ion battery stacks

Jingjuan Chen · Hongfa Xiang · Le Zhang · Haihui Wang

Received: 14 January 2012 / Accepted: 23 April 2012 / Published online: 11 May 2012

Abstract An integrative cell with a porous Al_2O_3 membrane as both a support and a separator has been fabricated. $LiFePO_4$ and graphite were coated onto the both sides of the rigid porous Al_2O_3 separator, while an electrolyte was infiltrated inside. The $LiFePO_4$/graphite integrative cells were evaluated in coin-type cells and exhibited good cycle capacity. The self-standing integrative cell was a simple and promising technology to assemble the battery stacks and meanwhile had an obvious advantage of forming a firm structure, which could avoid inner short circuit during being moved or crashed.

Keywords Lithium-ion battery · Integrative cell · Separator · Inorganic membrane

1 Introduction

With fossil energy decreasing, the energy storage and conversion devices will play an increasing role in the future [1–3]. Lithium-ion batteries are the most attractive secondary batteries owing to their high energy density, long cycling lifetime, and low self-discharge rate [4–8]. The self-standing integrative cell, i.e., an integration of anode, cathode, separator, and electrolyte has been drawing great attentions because it needs no external support to maintain contact between the electrodes and the separator and it could prevent the cell from inner short circuit during being moved or crashed. Tarascon et al. [9, 10] suggested a self-standing battery stack supported by gel polymer electrolytes polyvinylidene fluoride (PVDF), poly(vinylidene fluoride co-hexafluoropropene) (PVDF-HFP) as an electrolyte material and was activated by filling the cell with a liquid electrolyte. To improve the ionic conductivities, mechanical and thermal stability of the self-standing battery stack, self-standing polymer electrolyte containing ceramic fillers such as nano-scale SiO_2 and Al_2O_3 was proposed [11–14]. Prosini et al. [15] prepared self-standing integrative lithium-ion cells using an intrinsically porous separator made of a PVDF-HFP matrix with Al_2O_3 as the filler. By introducing ceramic fillers such as Al_2O_3, the electrochemical properties of the self-standing battery have been improved. However, the polymer separators will distort or fuse at relatively high temperature (>100 °C) or be punctured by lithium dendrites produced during charge and discharge cycling, which lead to internal short circuit and serious security problems [16–18].

In our previous work [19], we found that the inorganic Al_2O_3 separators exhibit a higher ionic conductivity and electrolyte retention than the polymer separator. We also found that $LiFePO_4$/graphite cell with the Al_2O_3 porous separator possesses excellent electrochemical performance, which indicates that the porous Al_2O_3 separator was very promising to be applied in the lithium-ion batteries. In this paper, the porous Al_2O_3 membrane is used as both a separator and a support to fabricate a self-standing integrative cell. The self-standing integrative cell is made of both electrodes materials adhered onto the rigid porous Al_2O_3 membrane with a sandwich structure, which is subsequently activated by infiltrated with a liquid electrolyte of 1 M $LiPF_6$/ethylene carbonate (EC) + dimethyl carbonate (DMC) (1:1 v/v). The integrative cell can hold adequate electrolyte to satisfy the requirement of more electrode materials than that of the cell with the polymer separators

J. Chen · H. Xiang · L. Zhang · H. Wang (✉)
School of Chemistry & Chemical Engineering,
South China University of Technology, Guangzhou 510640,
Guangdong, China
e-mail: hhwang@scut.edu.cn

because the inorganic Al_2O_3 porous membrane possesses excellent performance in electrolyte absorption and retention. Furthermore, the battery stack with desired capacity and voltage can be adjusted by plugging integrative cells into framework. Such battery stacks are convenient to manufacture, manage, and maintain because they are composed of intact self-standing cells that can be plugged in and drawn out separately.

2 Experimental

The porous Al_2O_3 separators were prepared by a double sintering process as described in our previous work [19]: micro-size alumina (300 mesh), nano-sized Al_2O_3 powder (Qingdao Xinhai Ltd. Co.), and ethylene diamine tetraacetic acid (EDTA) as a pore-forming agent were mixed at the mass ratio of 3:3:4. Platelets (Φ 16 mm) were pressed at a pressure of 10 Mbar and sintered at 1,000 °C for 5 h in air. Porous Al_2O_3 platelets were formed by removing EDTA after sintering at 1,000 °C. Then, the sintered porous platelets were rinsed and ultrasonicated in ethanol for 5 min to remove some separated particles from the pores. After being dried in a vacuum oven for 12 h, the sintered porous Al_2O_3 platelets were re-sintered at 1,500 °C for 5 h to get the final inorganic separators. The cathode electrode materials consisting of 70 wt% $LiFePO_4$ (Tianjin STL Co. Ltd.), 10 wt% acetylene black, and 20 wt% PVDF powder, and the anode electrode materials consisting of 80 wt% graphite (Hitachi Powdered Metals Co. Ltd.) and 20 wt% PVDF powder were dispersed in *N*-methyl-2-pyrrolidone (NMP) to form slurries. Then, the resultant slurries were uniformly pasted on either side of the porous Al_2O_3 separator with a blade and dried at 120 °C for 10 h in a vacuum oven (DZF-6020, Shanghai Qi Xin Scientific Instrument Co., Ltd., China) to form the self-standing integrative cell. Finally, the electrolyte of 1 M $LiPF_6$/EC + DMC (1:1 v/v) was infiltrated into the integrative cell. The electrode area is 1.70 cm^2.

The self-standing integrative cells were assembled in CR2032 coin-type cells in an argon-filled glove box (Mikrouna). Cyclic voltammetry (CV) measurements were carried out on an electrochemical workstation (Zahner IM6ex) over the potential range 2.40–4.30 V at a scanning rate of 0.2 mV s^{-1}. Impedance measurements were also performed on the electrochemical workstation (Zahner IM6ex) in a frequency range from 1 MHz to 100 mHz with ac signal amplitude of 10 mV. The charge–discharge cycle was performed at 0.1 C in the voltage range of 2.4–4.3 V using a Battery Testing System (Shenzhen Neware Electric Co., Ltd. China). Herein, 0.1 C means that it takes 10 h for the cell to charge or discharge in a predefined voltage window. All the cell tests were carried out at room temperature.

3 Results and discussion

Figure 1 shows the schematic diagram of integrative cell preparation process. As shown in Fig. 1, the cathode and anode slurries were uniformly pasted on either side of the porous Al_2O_3 separator with a blade to form the self-standing integrative cell after infiltrated the electrolyte. The integrative cell can significantly simplify the battery manufacture process due to the rigidity of the Al_2O_3 separator [20]. More importantly, a battery stack can be composed by the self-standing integrative cells through plugging the self-standing integrative cells into the grooves which are designed with appropriate circuits to realize the series and/or parallel connection among the units. The stack will possess sufficient rigidity and strength so that it can be encapsulated without any extra support which is necessary for the common battery with polymer separator [20]. Furthermore, such battery stacks are convenient to manufacture, manage, and maintain because the independent self-standing cells can be plugged in and drawn out separately, which provides a novel design for battery, especially large-scaled storage battery.

Figure 2a presents the photograph of the as-prepared self-standing integrative unit. As shown in Fig. 2a, the thickness of the self-standing integrative unit is about 300 μm with a 200 μm separator. The electrode materials are adhered on the surface of the porous separator without infiltrating into the pores of the separator. Figure 2b shows the SEM image of the prepared Al_2O_3 separator. As shown in Fig. 2b, the Al_2O_3 particles with the size of 200–500 nm have been successfully sintered and the clear and homogeneous pores with the size of several hundred nanometers have been formed. The porosity of the Al_2O_3 separator is estimated to be around 70 % based on the geometrical volume of the separator plate and the actual volume of the solid (the ratio of mass and the density of ~4 g cm^{-3}), which is much higher than that of polymer separators (~40 %) [19]. Although the porosity of 70 % is quite high, the separator still has sufficient mechanical strength owing to the solid bonding caused by re-sintering at 1,500 °C.

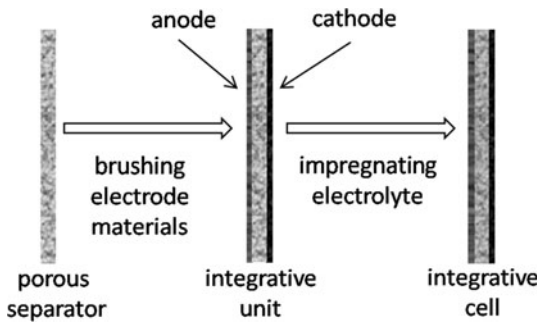

Fig. 1 Schematic diagram of integrative cell preparation

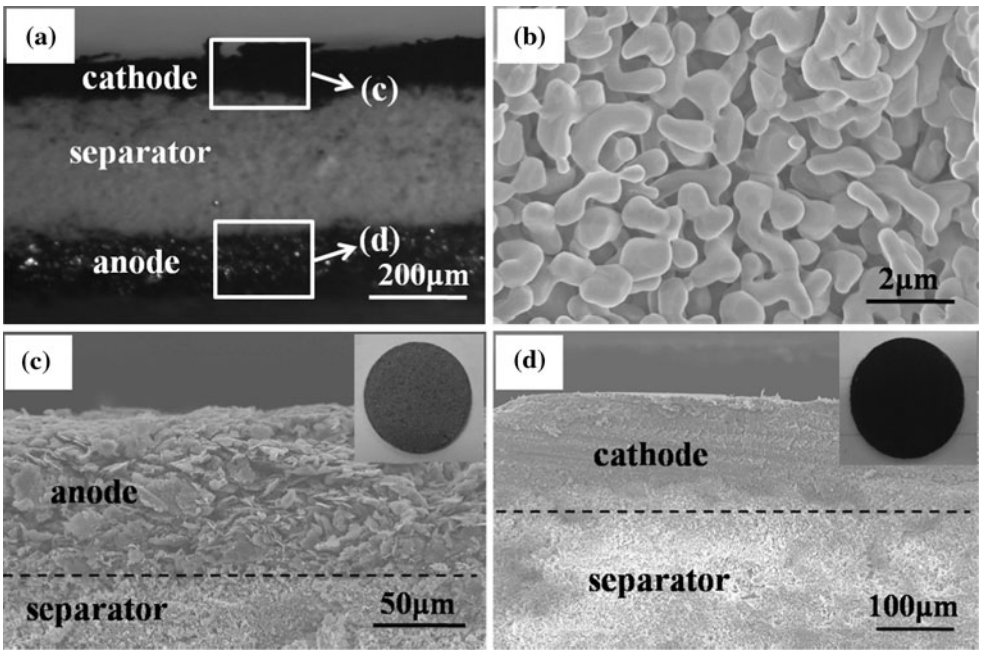

Fig. 2 **a** The *photograph* of prepared self-standing sandwich unit. **b** SEM images of the porous Al_2O_3 separator. **c**, **d** Images of the *areas marked* in (**a**) respectively, the *inset* of (**c**) and (**d**) are the photographs of the electrodes

The interfaces between both the electrodes and the separator are shown in Fig. 2c, d, respectively. As shown in Fig. 2c, d, both electrode materials are tightly adhered on the separator because the surface of Al_2O_3 membrane is porous and rough. Inner short circuit during being moved or crashed that would occur in common batteries with electrode materials piled or wound with the separator can be avoided by such integrative structure. The separator serves as a support to avoid the external support to the rigidity of the cell. At the same time, external press which is needed for the common cells can be left out due to the toughly contact between the electrode materials and the separator.

The CV curves of the integrative cell are shown in Fig. 3. The weak peak at 2.83 V in the initial cycle corresponds to the formation of solid electrolyte interphase (SEI) layer [21, 22]. Obviously, only one main peak pair of an anodic peak at 3.73 V and a cathodic peak at 2.92 V, which corresponds to the two-phase charge/discharge reaction of the Fe^{3+}/Fe^{2+} redox couple was observed [23]. Although the intensity and integral areas of the main peaks slightly become low with cycling, the potentials of the oxidation and reduction peaks did not change, which demonstrates that the electrochemical reaction in the integrative battery is reversible [21].

Cycling performances of the integrative cell are examined by charge and discharge tests. The cell is galvanostatically cycled between 2.4 and 4.3 V at 0.1 C. Fig. 4 presents the charge–discharge curves of the integrative cell during the first three cycles. The flat voltage plateau at

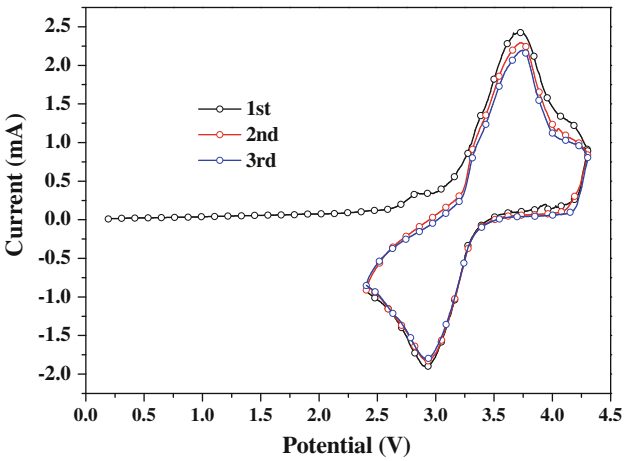

Fig. 3 Cyclic voltammetry (CV) curves of the $LiFePO_4$/graphite integrative cell (Scan rate: 0.2 mV s^{-1}; scan range: 2.4–4.3 V)

3.1–3.3 V range indicates the two-phase nature of the lithium extraction and insertion reactions between $LiFePO_4$ and $FePO_4$ [23]. The coulombic efficiency in the first cycle is 74 %, and the irreversible capacity is associated with the formation and growth of lithium-consuming SEI layer [24–26], and then the coulombic efficiencies increase to more than 90 % in the following two cycles.

Figure 5 shows the cycling performance of the integrative cell. When the contents of PVDF are 10 % in cathode and anode mixtures, the discharge capacity gradually decays from 88.7 mAh g^{-1} (1st cycle) to 64.2 mAh g^{-1} (20th cycle), as shown in Fig. 5a. However, when the

contents of PVDF are increased to 20 % in cathode and anode mixtures, the discharge capacity rises gradually from 121.4 mAh g^{-1} (1st cycle) to 150 mAh g^{-1} (7th cycle), then keeps stable in subsequent cycles, as shown in Fig. 5b. The obvious capacity fading may be mainly caused by peeling off of the electrode materials from the separator and more binder added can restrain electrode materials peeling off from the separator, which is beneficial for the performance of the cell. Electrochemical impedance spectra (EIS) were carried out to evaluate the electrochemical kinetics properties of the as-prepared integrative cells. Figure 6 shows the Nyquist plots of the experimental data and fitting results of the unused $LiFePO_4$/graphite integrative cell and the cell after 3 cycles at 30 % SOC (state of charge) with the dc potential of 3.31 V. Each of the spectra separates consists of a high frequency region

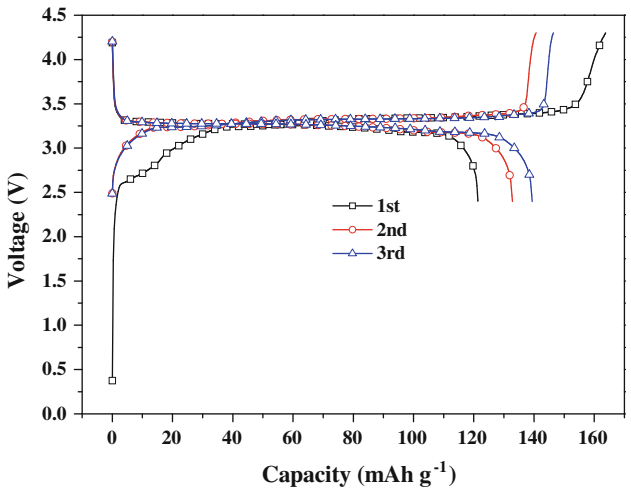

Fig. 4 The charge–discharge curves for the first three cycles of the $LiFePO_4$/graphite integrative cell (voltage range: 2.4–4.3 V)

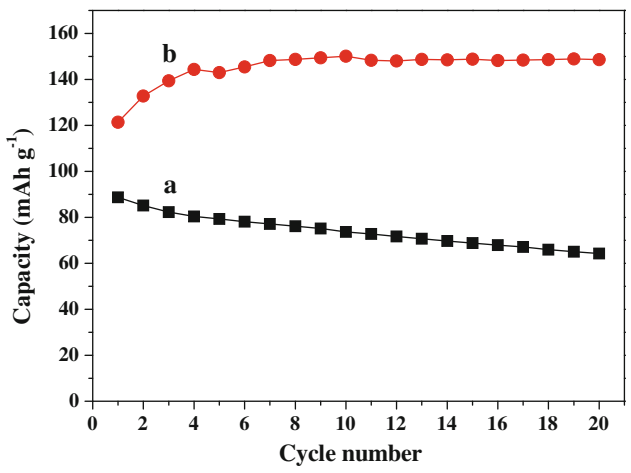

Fig. 5 Cycle capacity of the integrative cell, *a* with 10 % PVDF in both cathode and anode mixtures, *b* with 20 % PVDF in both cathode and anode mixtures; (voltage range: 2.4–4.3 V at a rate of 0.1 C)

(a semicircle) and a low frequency region (a straight line). The high frequency region of the semicircle represents the migration of the Li^+ ions at the electrode/electrolyte interface through the solid electrolyte interface (SEI) layer. The low frequency region of the straight line is attributed to the diffusion of the lithium-ions into the bulk of the electrode material, which was called Warburg diffusion [27–30]. The fitting results were obtained by ZsimpWin software using an equivalent circuit shown in Fig. 6, where R_e represents the Ohmic resistance of the research system, including the Ohmic resistance of the electrolyte, the electrode, the interface, etc., constant phase element (CPE) represents the double layer capacitance and the SEI film capacitance instead of a capacitor to compensate for non-homogeneity in the system, R_{ct} is the charge transfer resistor, and W_s is the finite length Warburg with a short circuit terminus [27, 28]. The parameters obtained by fitting are listed in Table 1. As shown in Table 1, R_e value of $LiFePO_4$/graphite integrative cell after 3 cycles (17.49 Ω) is higher than that of the unused cell (11.77 Ω), indicating the Ohmic resistance increasing during the cycling, which was possibly due to the swelling of the PVDF. It must be

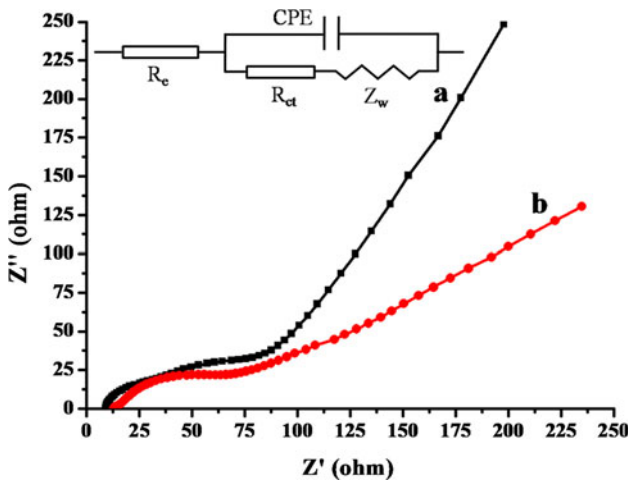

Fig. 6 Nyquist plots for the $LiFePO_4$/graphite integrative cell with 20 % PVDF and equivalent circuit for EIS data fitting (*subfigure*) *a* unused, *b* after 3 cycles at SOC = 30 % (amplitude potential of 10 mV; frequency ranging: 1 MHz to 100 mHz)

Table 1 EIS fitting results of pristine $LiFePO_4$/graphite integrative cell and the cell after 3 cycles

Parameter	Pristine integrative cell	Integrative cell after 3 cycles
R_e (Ω)	11.77	17.49
R_{ct} (Ω)	2.573	11.93
CPE (μF)	23.19	54.47
W_s (Ω)	1196	308.0

pointed out that the integrated battery is far from being optimized in terms of the overall geometrical configuration and the capacities balance between the two electrodes.

4 Conclusion

The self-standing integrative cell with electrode materials coated onto the porous Al_2O_3 separator had been fabricated. As the integrative cell was supported by rigid porous Al_2O_3 membrane, it could be simply encapsulated after infiltrated with electrolyte. The capacity of the $LiFePO_4$/graphite integrative battery was 150 mAh g^{-1} (7th cycle), then keeps stable during 20 cycles. Such self-standing integrative cell with Al_2O_3 porous separator could provide a competitive candidate to the currently rolling battery assembly, especially for large-sized energy storage device.

Acknowledgments This study was supported by National Science Foundation of China (Grant No. 21006033), Program for New Century Excellent Talents in Chinese Ministry of Education (No. NECT-07-0307) and the Fundamental Research Funds for the Central Universities, SCUT (2009220038).

References

1. Mulder G, De Ridder F, Six D (2010) Sol Energy 84:1284
2. Divya KC, Østergaard J (2009) Electr Power Syst Res 79:511
3. Elhadidy MA, Shaahid SM (1999) Renew Energy 18:77
4. Hoff TE, Perez R, Margolis RM (2007) Sol Energy 81:940
5. Qian H, Zhang J, Lai J-S, Yu W (2011) IEEE Trans Power Electron 26:886
6. Hall PJ, Bain EJ (2008) Energy Policy 36:4352
7. Henson W (2008) J Power Sources 179:417
8. Tarascon JM, Armand M (2001) Nature 414:359
9. Du Pasquier A, Tarascon J-M (2001) US Patent 5418091
10. Du Pasquier A, Amatucci GG, Plitz I, Zheng T, Gozdz AS, Tarascon J-M (2000) Solid State Ion 135:249
11. Lee K-H, Lee Y-G, Park J-K, Seung D-Y (2000) Solid State Ion 133:257
12. Appetecchi GB, Romagnoli P, Scrosati B (2001) Electrochem Commun 3:281
13. Rajendran S, Mahendran O, Kannan R (2002) J Phys Chem Solids 63:303
14. Jeong H-S, Kim D-W, Jeong YU, Lee S-Y (2010) J Power Sources 195:6116
15. Prosini PP, Villano P, Carewska M (2002) Electrochim Acta 48:227
16. Zhang SS (2007) J Power Sources 164:351
17. Djian D, Alloin F, Martinet S, Lignier H, Sanchez JY (2007) J Power Sources 172:416
18. Zhang HP, Zhang P, Li ZH, Sun M, Wu YP, Wu HQ (2007) Electrochem Commun 9:1700
19. Xiang HF, Chen JJ, Li Z, Wang HH (2011) J Power Sources 196:8651
20. Mohamed M, Ishikawa H, Uchida I (2004) J Appl Electrochem 34:1103
21. Persi L, Croce F, Scrosati B (2002) Electrochem Commun 4:92
22. Zhang Y, Wang C-Y, Tang X (2011) J Power Sources 196:1513
23. Takahashi M (2002) Solid State Ion 148:283
24. Shim J, Striebel KA (2003) J Power Sources 119:955
25. Chang HH, Chang CC, Su CY, Wu HC, Yang MH, Wu NL (2008) J Power Sources 185:466
26. Shi HC, Cho WI, Jang H (2006) Electrochim Acta 52:1472
27. Feng Y (2010) Mater Chem Phys 121:302
28. Yang KR, Deng ZH, Suo JS (2012) J Power Sources 201:274
29. Wolfenstine J, Allen JL (2008) J Power Sources 180:582
30. Shenouda AY, Murali KR (2008) J Power Sources 176:332